Journal of Power Sources 271 (2014) 60–64

Contents lists available at ScienceDirect

Journal of Power Sources

journal homepage: www.elsevier.com/locate/jpowsour

Short communication

Synthesis, structure and lithium ionic conductivity of solid solutions of $Li_{10}(Ge_{1-x}M_x)P_2S_{12}$ (M = Si, Sn)

Yuki Kato [a, b, *], Ryoko Saito [c], Mitsuru Sakano [c], Akio Mitsui [d], Masaaki Hirayama [b], Ryoji Kanno [b]

[a] Battery Research Div., Higashifuji Technical Center, Toyota Motor Corporation, 1200 Mishuku, Susono, Shizuoka 410-1193, Japan
[b] Department of Electronic Chemistry, Interdisciplinary Graduate School of Science and Engineering, Tokyo Institute of Technology, 4259 Nagatsuta, Midori, Yokohama 226-8502, Japan
[c] Advanced Material Engineering Div., Higashifuji Technical Center, Toyota Motor Corporation, 1200 Mishuku, Susono, Shizuoka 410-1193, Japan
[d] Material Engineering Management Div., Material Analysis Dept., Toyota Motor Corporation, 1200 Mishuku, Susono, Shizuoka 410-1193, Japan

HIGHLIGHTS

- The mixed cation system, $Li_{10}(Ge_{1-x}M_x)P_2S_{12}$ (M = Si, Sn), was synthesized.
- Single phase of $Li_{10}GeP_2S_{12}$ (LGPS)-type crystal was obtained.
- The maximum conductivity of 8.6 mS cm^{-1} was obtained at $Li_{10}Ge_{0.95}Si_{0.05}P_2S_{12}$.
- The lattice volume is not the only parameter that affects the ionic conduction.

GRAPHICAL ABSTRACT

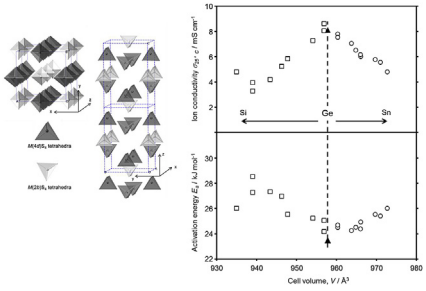

ARTICLE INFO

Article history:
Received 1 July 2014
Received in revised form
22 July 2014
Accepted 23 July 2014
Available online 12 August 2014

Keywords:
All-solid-state battery
Lithium ionic conductor
$Li_{10}GeP_2S_{12}$
LGPS
Solid solution

ABSTRACT

The mixed cation system, $Li_{10}(Ge_{1-x}M_x)P_2S_{12}$ (M = Si, Sn), was synthesized and the ionic conductivities of the resulting solid solutions were determined. The Si–Ge and Ge–Sn systems provided single phase solid solutions for the composition $0 \le x < 1.0$ and $0 \le x \le 1.0$ in $Li_{10}(Ge_{1-x}Si_x)P_2S_{12}$ and $Li_{10}(Ge_{1-x}Sn_x)P_2S_{12}$, respectively. The lattice size gradually increased from Si to Sn through the Ge systems, reflecting the ionic size of these elements. On the other hand, conductivity did not follow the increase in lattice volume. Conductivity increased in the Si to Ge system, with the maximum conductivity value of 8.6×10^{-3} S cm^{-1} provided by the compressed powder with the composition $Li_{10}Ge_{0.95}Si_{0.05}P_2S_{12}$, which is close to the original $Li_{10}GeP_2S_{12}$ (LGPS) composition. The conductivity decreased with increasing Sn content, indicating that lattice volume is not the only parameter that affects ionic conduction in this structure. The relationship between conductivity and lattice volume is discussed.

1. Introduction

Large-scale batteries are in high demand [1,2] for applications such as plug-in electric hybrid or electric vehicles, and smart electric power grids. The all-solid-state battery is the most promising candidate for future battery systems, due to the high energy density obtaining by direct-series-stacking of the battery cells [3]. However, their current low power density remains a major issue to be solved, and is caused by the high resistivity of the solid electrolyte. To overcome this problem, the past few decades have seen an ongoing search to find new solid electrolyte materials [4–9]. The lithium superionic conductor, $Li_{10}GeP_2S_{12}$, shows an extremely high lithium ionic conductivity of 12 mS cm^{-1} at 27 °C [10], which is

* Corresponding author. Battery Research Div., Higashifuji Technical Center, Toyota Motor Corporation, 1200 Mishuku, Susono, Shizuoka 410-1193, Japan. Tel./fax: +81 55 997 9661.
E-mail address: yuki_katoh@mail.toyota.co.jp (Y. Kato).

http://dx.doi.org/10.1016/j.jpowsour.2014.07.159
0378-7753/

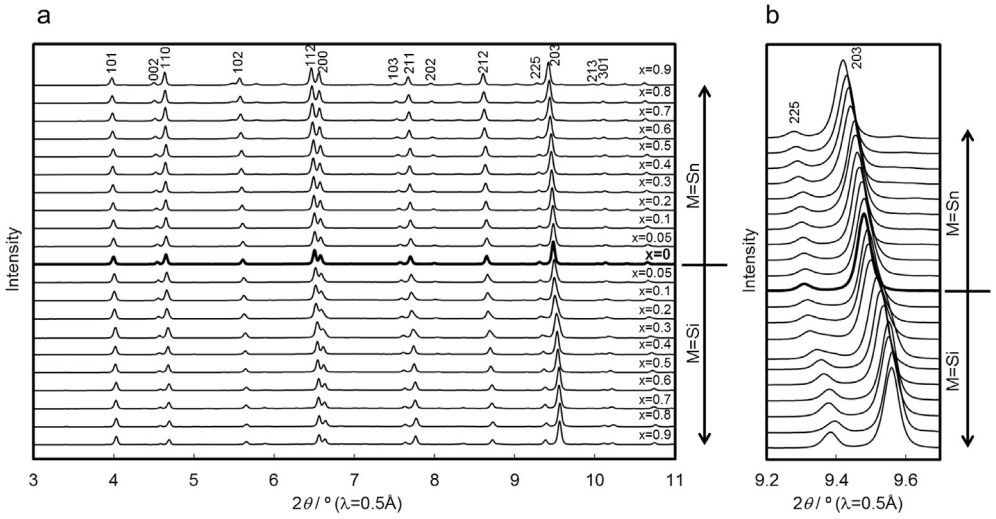

Fig. 1. X-ray diffraction patterns of $Li_{10}(Ge_{1-x}M_x)P_2S_{12}$ (M = Si, Sn).

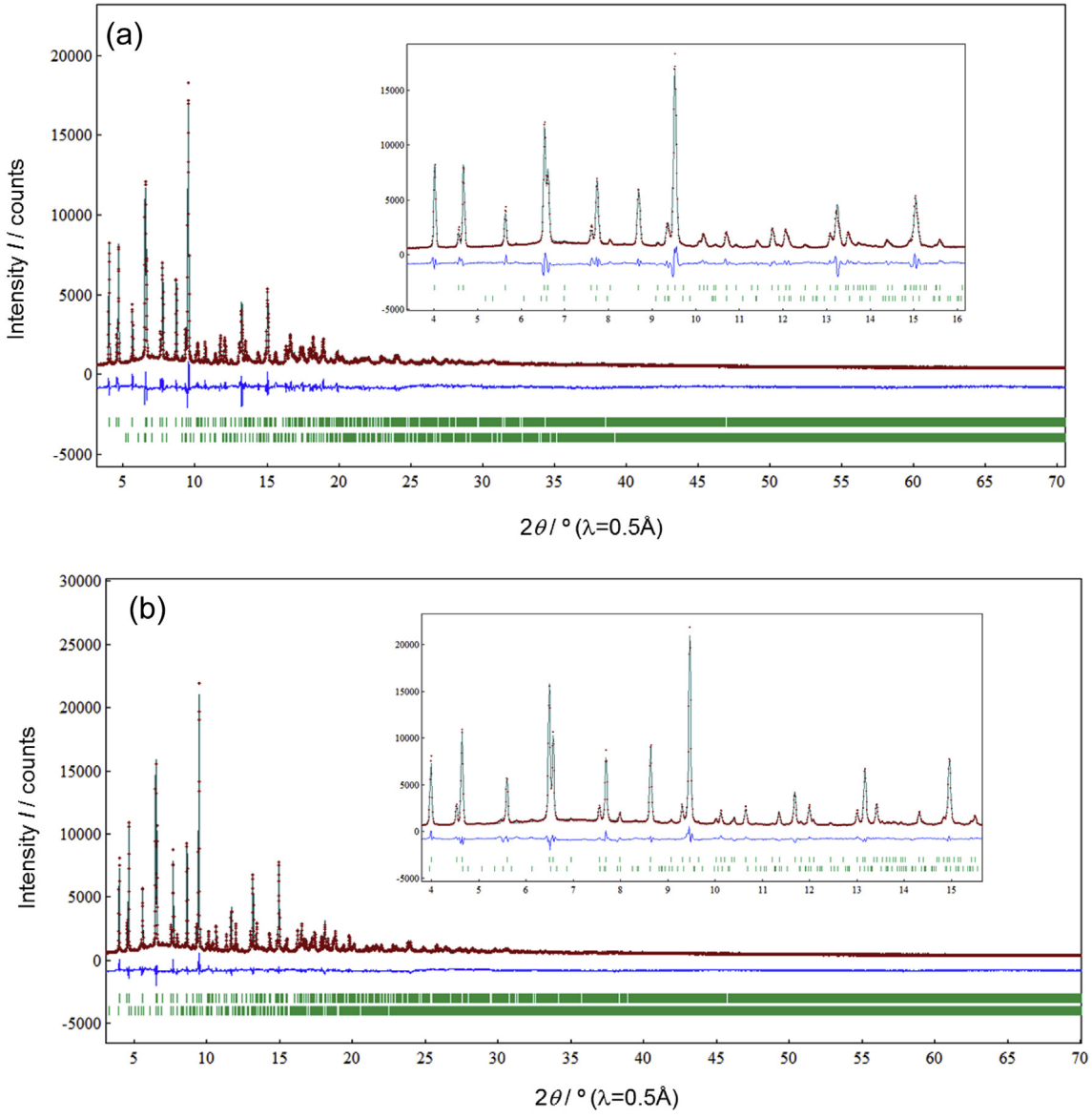

Fig. 2. Rietveld refinement pattern of $Li_{10}(Ge_{0.7}Si_{0.3})P_2S_{12}$ (a) and $Li_{10}(Ge_{0.7}Sn_{0.3})P_2S_{12}$ (b).

comparable to or higher than the conductivities of practical organic liquid electrolytes used in lithium-ion batteries. The conduction mechanism has been studied based on the method of first principles calculations, and a suitable lattice size for lithium ion conduction has been proposed [11–13]. Furthermore, cation substitutions of Ge to Si or Sn have been examined [14,15]; $Li_{10}SnP_2S_{12}$ with the $Li_{10}GeP_2S_{12}$ (LGPS) type structure showed a conductivity value of 4 mS cm^{-1} at room temperature [14]. The existence of Sn analogues indicates a whole range of solid solution compositions between the Ge and Sn systems, which may provide information on lattice volume and ionic conduction. Furthermore, an electrolyte containing less Ge might be more practical, given the high cost of germanium.

In the present study, the effect of lattice size on ionic conductivity was investigated for Sn and Si substituted systems with the LGPS-type structure. Solid solutions of $Li_{10}(Ge_{1-x}M_x)P_2S_{12}$ (M = Si, Sn) were synthesized and the crystal structures were determined by synchrotron X-ray diffraction analysis. The relationship between the structure and ionic conductivity is discussed.

2. Experimental

The starting materials Li_2S (Nippon Chemical Industrial), P_2S_5 (Aldrich), SiS_2 (Alfa) GeS_2 (Kojundo Chemicals) and SnS_2 (Kojundo Chemicals) were mixed in an appropriate molar ratio in an argon-filled glove box. The mixture was put into a ZrO_2 pot together with ZrO_2 balls (ϕ10 mm), the mixture was mechanically milled using a planetary ball milling apparatus at 370 rpm for 40 h, and then the mixture was put into a quartz tube and heated at 550 °C for 8 h. The X-ray amorphous specimens obtained by ball milling were crystallized to the LGPS-type crystal by heat treatment.

X-ray diffraction patterns of the powdered samples were obtained using the high flux synchrotron X-ray source at the beam line BL19B2 at the SPring-8 facility. A Debye–Scherrer diffraction camera was used for the measurements. The specimen was sealed in a quartz tube (approximately 0.5 mm diameter) under vacuum for XRD measurements. Diffraction data were collected in 0.01° steps from 3° to 78° in 2θ. The incident-beam wavelength was calibrated using a NIST SRM Ceria 640b CeO_2 standard and was fixed at 0.4993 Å. The program RIETAN-FP [16] was used for Rietveld refinement of the structure. Very small peaks due to trace impurities were observed in the diffraction patterns, and these peaks were indexed by the β-Li_3PS_4-type phase [17].

Ionic conductivities of the compressed powder were measured under a pressure of 420 MPa. The AC impedance was measured between −30 and 60 °C in an argon atmosphere in the frequency range of 0.1 Hz to 1 MHz using a frequency response analyzer (Solarton, 1260). The conductivity data were obtained from the impedance plots of the data. The conductivity of the compressed power of $Li_{10}GeP_2S_{12}$ was 8 mS cm^{-1}, slightly lower than the conductivity value of 12 mS cm^{-1} obtained for sintered $Li_{10}GeP_2S_{12}$, indicating that the grain boundary contribution is not significant for the total conductivity value.

Table 1
Structural parameters of $Li_{10}(Ge_{0.7}Si_{0.3})P_2S_{12}$.

Atom	Site	g	x	y	z	B
Li(1)	16*h*	0.671(9)	0.2568(7)	0.2758(1)	0.2070(1)	8.6481(4)
Li(2)	4*d*	1	0	0.5	0.9399(8)	4.7263(9)
Li(3)	8*f*	0.312(11)	0.2406(8)	=*y*(Li(3))	0	7.8409(4)
Li(4)	4*d*	0.668(3)	0.0	0	0.2554(8)	5.1384(2)
Si(1)	4*d*	0.143(2)	0	0.5	0.6889(1)	0.3075(7)
Ge(1)	4*d*	0.356(9)	=*x*(Si(1))	=*y*(Si(1))	=*z*(Si(1))	=*B*(Si(1))
P(1)	4*d*	1 − g(Ge(1)−g(Si(1))	=*x*(Si(1))	=*y*(Si(1))	=*z*(Si(1))	=*B*(Si(1))
Si(2)	2*b*	0	0	0	0.5	=*B*(Si(1))
Ge(2)	2*b*	0	=*x*(Si(2))	=*y*(Si(2))	=*z*(Si(2))	=*B*(Si(1))
P(2)	2*b*	1	=*x*(Si(2))	=*y*(Si(2))	=*z*(Si(2))	=*B*(Si(1))
S(1)	8*g*	1	0	0.1907(3)	0.4059(6)	2.995(5)
S(2)	8*g*	1	0	0.2960(1)	0.0976(9)	1.7988(1)
S(3)	8*g*	1	0	0.6978(3)	0.7934(6)	=*B*(S(2))

Unit cell: tetragonal $P4_2/nmc$ (137); a = 8.6799(2) Å, c = 12.579(3) Å, V = 947.73(7) Å^3; R_{wp} = 7.653, R_p = 1.41, Rb = 6.044, R_R = 22.095, Re = 3.760, goodness of fit $S = R_{wp}/Re$ = 2.03; phase: β-Li_3PS_4 (ca. 6.0 mass%).

Table 2
Structural parameters of Li10(Ge0.7Sn0.3)P2S12.

Atom	Site	g	x	y	z	B
Li(1)	16*h*	0.536(5)	0.2494(3)	0.2754(2)	0.19110(2)	10.634(4)
Li(2)	4*d*	1	0	0.5	0.9394(12)	3.4830(11)
Li(3)	8*f*	0.373(9)	0.2422(5)	=*y*(Li(3))	0	7.695(3)
Li(4)	4*d*	0.662(8)	0.	0	0.272453(8)	6.473(7)
Ge(1)	4*d*	0.349(2)	0	0.5	0.6890(1)	0.3075(2)
Sn(1)	4*d*	0.128(7)	=*x*(Ge(1))	=*y*(Ge(1))	=*z*(Ge(1))	=*B*(Ge(1))
P(1)	4*d*	1 − g(Ge(1)−g(Sn(1))	=*x*(Ge(1))	=*y*(Ge(1))	=*z*(Ge(1))	=*B*(Ge(1))
Ge(2)	2*b*	0	0	0	0.5	=*B*(Ge(1))
Sn(2)	2*b*	0	=*x*(Ge(2))	=*y*(Ge(2))	=*z*(Ge(2))	=*B*(Ge(1))
P(2)	2*b*	1	=*x*(Ge(2))	=*y*(Ge(2))	=*z*(Ge(2))	=*B*(Ge(1))
S(1)	8*g*	1	0	0.1905(9)	0.4070(9)	2.0485(5)
S(2)	8*g*	1	0	0.2944(6)	0.0983(8)	1.316(8)
S(3)	8*g*	1	0	0.6994(8)	0.7915(2)	=*B*(S(2))

Unit cell: tetragonal $P4_2/nmc$ (137); a = 8.7300(7) Å, c = 12.659(3) Å, V = 964.81(7) Å^3; R_{wp} = 7.345, R_p = 5.577, Rb = 6.044, R_R = 21.011, Re = 3.724, goodness of fit $S = R_{wp}/Re$ = 1.97; phase: β-Li_3PS_4 (ca. 7.0 mass%).

3. Results and discussion

Fig. 1a shows the XRD patterns of the $Li_{10}(Ge_{1-x}M_x)P_2S_{12}$ (M = Si, Sn) synthesized in the present study. The main phases that appear in the patterns were indexed by the tetragonal crystal structure of $Li_{10}GeP_2S_{12}$ (space group $P4_2/nmc$ (137)) [10]. Additional peaks are observed for systems with a high level of Si or Sn substitution (large x values) in $Li_{10}(Ge_{1-x}M_x)P_2S_{12}$. These peaks were indexed by the orthorhombic unit cell of β-Li_3PS_4 (space group $Pnma$) [17]. No superlattice reflections of the LGPS type

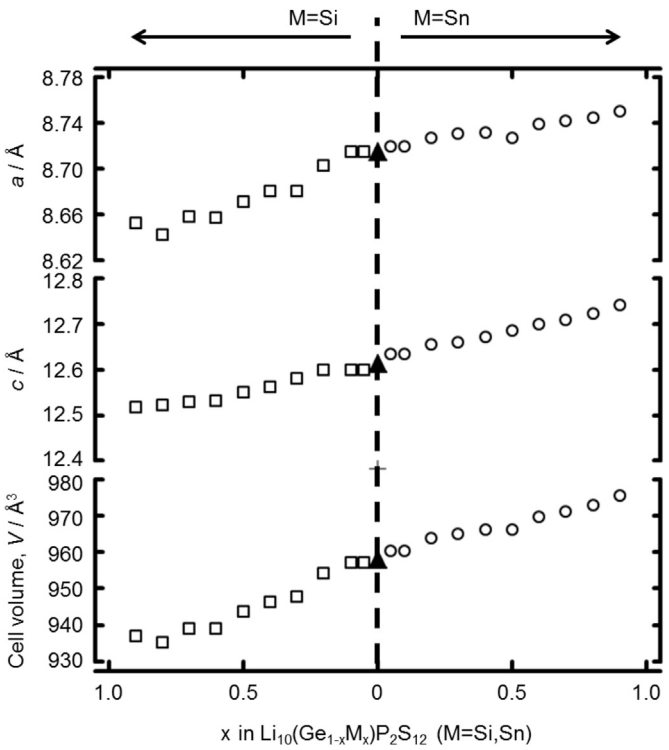

Fig. 3. Compositional dependence of the lattice parameters for $Li_{10}(Ge_{1-x}M_x)P_2S_{12}$ (M = Si, Sn).

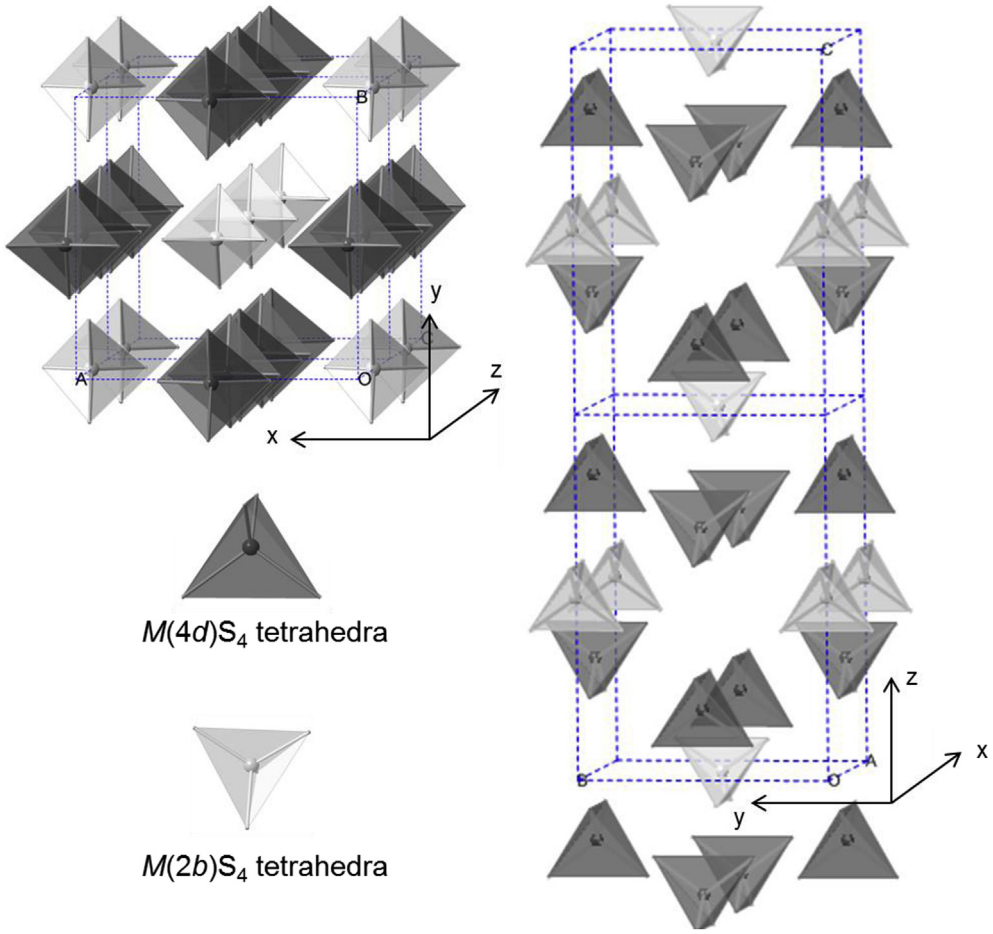

Fig. 4. Crystal structure of $Li_{10}(Ge_{1-x}M_x)P_2S_{12}$ (M = Si, Sn).

structure are observed for these X-ray diffraction patterns. The diffraction patterns show a continuous peak shift, as shown in Fig. 1b, which suggests formation of the solid solution with the composition $0 \leq x < 1.0$ and $0 \leq x \leq 1.0$ for $Li_{10}(Ge_{1-x}Si_x)P_2S_{12}$ and $Li_{10}(Ge_{1-x}Sn_x)P_2S_{12}$, respectively.

Fig. 2a and b shows the X-ray Rietveld refinement patterns of $Li_{10}(Ge_{1-x}Si_x)P_2S_{12}$ ($x = 0.3$) and $Li_{10}(Ge_{1-x}Sn_x)P_2S_{12}$ ($x = 0.3$), respectively. The structures were refined based on the structural data for $Li_{10}GeP_2S_{12}$ reported previously [10,18]. Tables 1 and 2 summarize the refined parameters. Fig. 3 shows the compositional dependence of the lattice parameters and volume in $Li_{10}(Ge_{1-x}M_x)P_2S_{12}$ (M = Si, Sn). The lattice parameters and cell volume changed with x; unit cell sizes increased when Ge was replaced with Sn and decreased when replaced with Si. Fig. 4 shows the crystal structure of $Li_{10}(Ge_{1-x}M_x)P_2S_{12}$ (M = Si, Sn). The structure consists of two sets of tetrahedra, M(4*d*)S_4 and M(2*b*)S_4; the 2*b* site is occupied only by P, which is consistent with the results obtained by powder neutron diffraction [10] and single crystal X-ray analyses [11,12,18]. The 4*d* site was occupied by either Si, Ge, Sn or P, and the occupancy varied with x in $Li_{10}(Ge_{1-x}M_x)P_2S_{12}$ (M = Si, Sn). The size of the tetrahedra changes with the ionic radius of the central cations. Therefore, the lattice parameter change shown in Fig. 3 might be due to the change in size of the M(4*d*)S_4 tetrahedra in the crystal structure.

Ionic conductivity was determined by AC impedance measurements. The impedance plots of the data consist of a semicircle and a spike; as the bulk and grain boundary contributions could not be separated, the conductivities were obtained as the sum of both contributions. The temperature dependence of the conductivities in $Li_{10}(Ge_{1-x}M_x)P_2S_{12}$ (M = Si, Sn) is shown in Fig. 5. The highest conductivity, 8.6 mS cm^{-1} at 25 °C, was obtained at $x = 0.05$ in $Li_{10}(Ge_{1-x}Si_x)P_2S_{12}$. Fig. 6 shows the cell volume dependence of the conductivities and activation energies. The conductivity increased continuously as the cell volume increased from 935.0 to 956.9 $Å^3$, and provided the highest conductivity value at 25 °C of 8.6 mS cm^{-1}. The lowest activation energy, 23.5 kJ mol^{-1}, is obtained at a cell volume of approximately 957 $Å^3$. The ionic conductivity decreased as the cell volume increased above 956.9 $Å^3$. This result indicates that the conductivity is related to the lattice volume, and the maximum conductivity value was obtained with a composition near that of the original germanium system.

According to the first principal calculation results, the Si-substituted material might exhibit higher ionic diffusion than the Ge and Sn materials [13]. The results also indicated that the conductivity changes with the lattice volume, with a larger lattice volume potentially showing larger ionic conductivity. This effect was also suggested for the anion-substituted systems: selenide materials might show much higher conductivities than the sulfide or oxide systems. However, these expectations for the Si, Ge, and Sn systems are not consistent with our experimental results from conductivity measurements on the compact powder samples. The synthesis reaction conditions and conductivity measurement conditions are the same for all the samples synthesized in the present study; consequently, the grain boundary contribution might not significantly affect the total conductivity. The conductivity of sintered pellets of $Li_{10}GeP_2S_{12}$ (12 mS cm^{-1}) was higher than that of $Li_{10}SnP_2S_{12}$ (*ca.* 4 mS cm^{-1} [14,19]), according with the results of compressed powder. And the conductivity of sintered $Li_{10}SnP_2S_{12}$

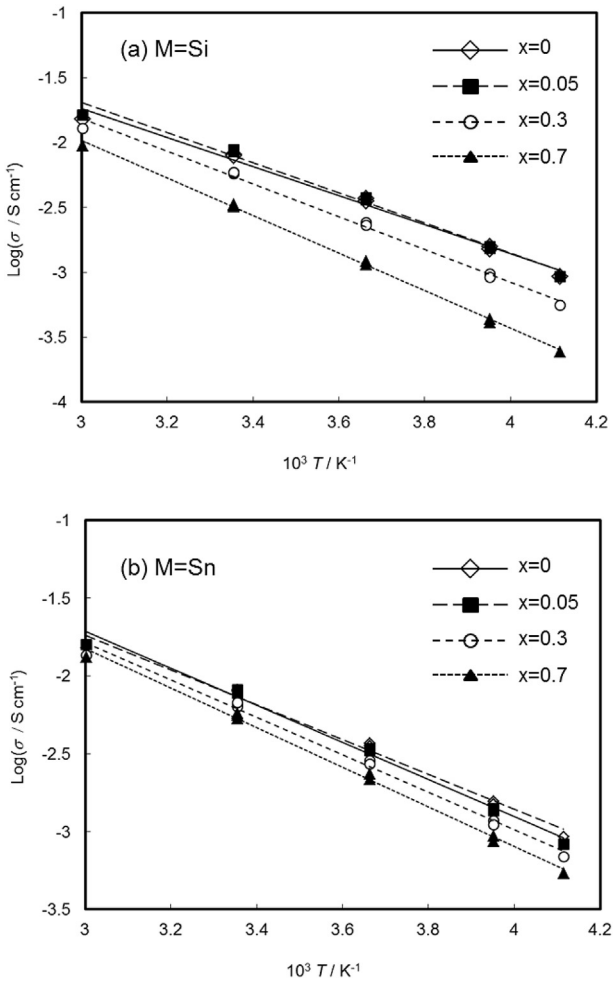

Fig. 5. Temperature dependence of the conductivity of $Li_{10}(Ge_{1-x}M_x)P_2S_{12}$ (M = Si, Sn).

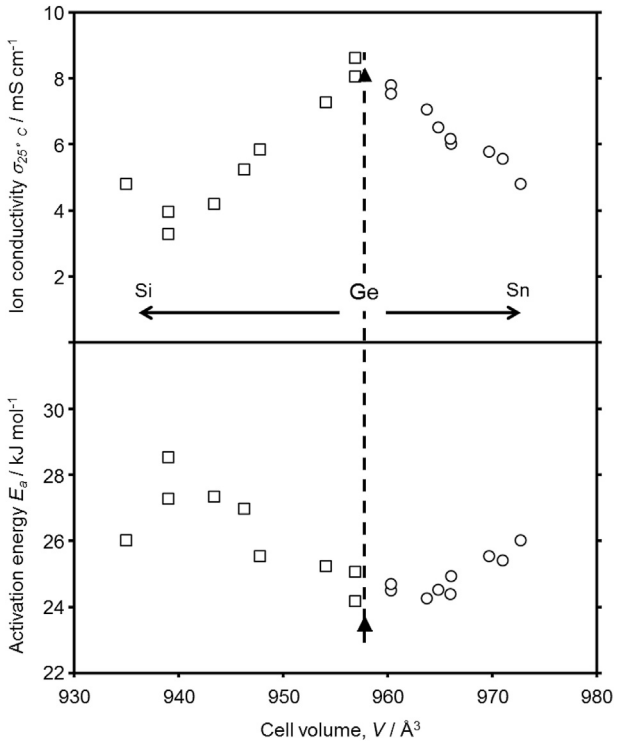

Fig. 6. Cell volume dependence of the conductivity and activation energy of $Li_{10}(Ge_{1-x}M_x)P_2S_{12}$ (M = Si, Sn).

was almost same with that of compressed powder state. Thus, the changes in the conductivity observed for the solid-solution systems are much larger than those expected from the grain-boundary contribution. Therefore, the rather low ionic conductivities of the Si and Sn systems might be intrinsic properties of the LGPS type materials. The increase in conductivity with decreasing x in $Li_{10}Ge_{1-x}Si_xP_2S_{12}$ could be explained by the decrease in lattice volume. On the other hand, the decrease in conductivity with increasing x in $Li_{10}Ge_{1-x}Sn_xP_2S_{12}$ cannot be understood based on expansion of the lattice alone. Further experimental studies on ionic mobility and the concentration of the mobile species are necessary to understand and identify the best compositions for high ionic conduction by the LGPS materials.

4. Conclusion

Solid solutions of $Li_{10}GeP_2S_{12}$-type host material with the composition $Li_{10}(Ge_{1-x}M_x)P_2S_{12}$ (M = Si, Sn) were systematically synthesized and their physical properties examined. The lattice parameters and volumes changed systematically with the replacement of M cations. The replaced Si and Sn ions occupied the 4*d* site of (Ge/P)S_4 tetrahedra. The maximum ionic conductivity was obtained with the approximate composition $x = 0.05$ in $Li_{10}(Ge_{1-x}Si_x)P_2S_{12}$. Although the lattice sizes gradually increased from the Si to Sn through to the Ge systems, the conductivity increased from the Si to the Ge system, and decreased with increasing Sn content. These results indicate that the lattice volume is not the only parameter that affects the ionic conduction of the structure. The results obtained by this work provide important suggestions for designing high ionic conductive solid electrolytes based on LGPS-type crystals, and are helpful for improving the characteristics of all-solid-state batteries.

Acknowledgements

The synchrotron radiation experiments were performed at the BL19B2 beam line at the SPring-8 facility with the approval of the Japan Synchrotron Radiation Research Institute (JASRI) (Proposal No. 2013A1768, 2013B1630). This work was supported in part by the Post Li-EAD project of the New Energy and Industrial Technology Development Organization (NEDO) of Japan.

References

[1] J.M. Tarascon, M. Armand, Nature 414 (2001) 359–367.
[2] M. Armand, J.M. Tarascon, Nature 451 (2008) 652–657.
[3] Y. Kato, K. Kawamoto, R. Kanno, M. Hirayama, Electrochemistry 80 (2012) 749–751.
[4] M. Tatsumisago, M. Nagao, A. Hayashi, J. Asian Ceram. Soc. 1 (2013) 17–25.
[5] Y. Inaguma, et al., Solid State Commun. 86 (1993) 689–693.
[6] R. Kanno, M. Murayama, J. Electrochem. Soc. 148 (2001) A742–A746.
[7] F. Mizuno, A. Hayashi, K. Tadanaga, M. Tatsumisago, Adv. Mater. 17 (2005) 918–921.
[8] S. Kondo, K. Takada, Y. Yamamura, Solid State Ionics 53 (1992) 1183–1186.
[9] K. Takada, N. Aotani, S. Kondo, J. Power Sources 43 (1993) 135–141.
[10] N. Kamaya, et al., Nat. Mater. 10 (2011) 682–686.
[11] Y. Mo, S.P. Ong, G. Ceder, Chem. Mater. 24 (2012) 15–17.
[12] S. Adams, R. Prasada Rao, J. Mater. Chem. 22 (2012), 7687–7619.
[13] S.P. Ong, et al., Energy Environ. Sci. 6 (2013) 148–156.
[14] P. Bron, et al., J. Am. Chem. Soc. 135 (2013) 15694–15697.
[15] A. Kuhn, et al., Condens. Matter Mater. Sci. (2014) arXiv:1402.4586.
[16] F. Izumi, K. Momma, Solid State Phenom. 130 (2007) 15–20.
[17] K. Homma, et al., Solid State Ionics 182 (2011) 53–58.
[18] A. Kuhn, J. Köhler, B.V. Lotsch, Phys. Chem. Chem. Phys. 15 (2013) 11620.
[19] S. Hori, K. Suzuki, M. Hirayama, Y. Kato, T. Saito, M. Yonemura, R. Kanno, Faraday Discussions (2014), in preparation.